Inorganic Chemistry

Article

Molecular and Electronic Structure of Square-Planar Gold Complexes Containing Two 1,2-Di(4-*tert*-butylphenyl)ethylene-1,2-dithiolato Ligands: [Au(²L)₂]¹⁺/⁰/¹⁻/²⁻. A Combined Experimental and Computational Study

Swarnalatha Kokatam,[†] Kallol Ray,[†] Joseph Pap,[†] Eckhard Bill,[†] William E. Geiger,[‡] Robert J. LeSuer,[‡] Philip H. Rieger,[§] Thomas WeyhermUller,[†] Frank Neese,[†] and Karl Wieghardt*,[†]

Max-Planck-Institut für Bioanorganische Chemie, Stiftstrasse 34-36, D-45470 Mülheim an der Ruhr, Germany, Department of Chemistry, University of Vermont, Burlington, Vermont 05405, and Department of Chemistry, Brown University, Providence, Rhode Island 02912

From the reaction of in situ generated 1,2-di(4-*tert*-butylphenyl)ethylene-1,2-dithiol, ²LH₂, and Na[AuCl₄]·2H₂O in 1,4-dioxane, green brown crystals of diamagnetic [N(*n*-Bu)₄][Au^{III}(²L)₂] (**1**) were obtained. As shown by cyclic voltammetry, **1** is a member of an electron-transfer series comprising the dianion [Au^{II}(²L)₂]²⁻, the monoanion [Au^{III}(²L)₂]⁻, the neutral species [Au^{III}(²L•)(²L)]⁰ ↔ [Au^{III}(²L)(²L•)]⁰, and the monocation [Au^{III}(²L•)₂]⁺. (²L•)¹⁻ represents the π radical anion ($S_{rad} = {}^1/_2$) of the one-electron oxidized closed-shell dianion (²L)²⁻. Oxidation of **1** in CH₂Cl₂ with ferrocenium hexafluorophosphate affords green, paramagnetic microcrystals of [Au^{III}(²L•)(²L)] ↔ [Au^{III}(²L)(²L•)] (**2**) ($S = {}^1/_2$). Complexes **1** and **2** have been characterized by X-ray crystallography. Both species possess square-planar monoanions and neutral molecules, respectively. From the oxidation reaction of **1** or [N(*n*-Bu)₄][Au^{III}(³L)₂] with 2–3 equiv of [NO]BF₄ in CH₂Cl₂, a green solution of [Au^{III}(²L•)₂]⁺ and green microcrystals of [Au^{III}(³L•)₂]BF₄ (**3**) were obtained, respectively; (³L)²⁻ represents the dianion 1,2-di(4-diphenyl)ethylene-1,2-dithiolate, and (³L•)¹⁻ is its π radical monoanion. The electronic structures of this series of gold species have been elucidated by UV–vis, EPR spectroscopies, and DFT calculations. It is shown computationally by density functional theoretical (DFT) methods that the electronic structure of [Au^{III}(¹L•)₂]⁺ is best described as a singlet diradical ($S_t = 0$); the ligand mixed valency in the neutral species **2** is of class (III) (delocalized); the monoanion in **1** contains a Au^{III} ion and two closed-shell dianionic ligands; and the corresponding dianions [Au(L)₂]²⁻ are best described as an intermediate Au^{II}/Au^{III} species with a metal–ligand delocalized SOMO (25% Au 5d, 75% 3p of four S atoms). (¹L)²⁻ is the dianion 1,2-di(phenyl)ethylene-1,2-dithiolate, and (¹L•)¹⁻ is the π radical monoanion. The neutral species [Pd^{II}(²L•)₂] (**4**) has also been synthesized and characterized by X-ray crystallography. Its electronic structure is the same as described for [Au^{III}(¹L•)₂]⁺ (singlet diradical), whereas that of the monoanion [Pd^{II}(²L•)(²L)]⁻ ↔ [Pd(²L)(²L•)]⁻ corresponds to that of the neutral gold complex **2**. Anodic oxidation of the analogous monoanion [Au^{III}(mnt)₂]⁻, where mnt = maleonitriledithiolate, gave the neutral complex [Au(mnt)(mnt•)] ($E_{1/2}$ = 0.91 V vs Fc⁺/Fc). The optical and EPR spectroscopies of [Au(mnt)(mnt•)] were consistent with those observed for the corresponding di(*tert*-butylphenyl)-ethylenedithiolate complex **2**.

Introduction

Square-planar bis(dithiolene)gold complexes, [Au(L)₂]ⁿ (*n* = 0, 1−, 2−), have been investigated in depth in the past, and their structural and spectroscopic properties have been

reported.[1] (In this paper, we will designate specific dithiolene ligands as (*ᵐ*L)²⁻ or (*ᵐ*L•)¹⁻ with *m* = 1, 2, or 3, whereas simple (L) is a generic representation of dithiolene ligands irrespective of their oxidation level.) The majority of these species are diamagnetic, monoanionic [Au^{III}(L)₂]⁻ complexes that possess a central diamagnetic Au(III) ion with a d⁸

* To whom correspondence should be addressed. E-mail: wieghardt@mpi-muelheim.mpg.de.
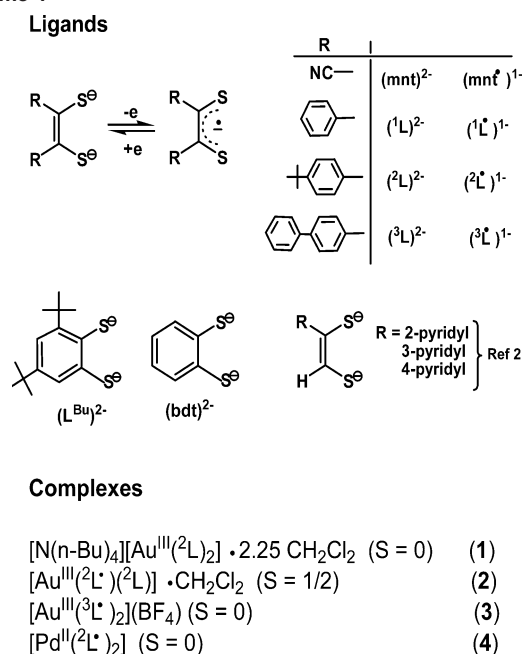† Max-Planck-Institut für Bioanorganische Chemie.
‡ University of Vermont.
§ Brown University.

(1) Dithiolene Chemistry. Stiefel, E. I., Ed. *Progr. Inorg. Chem.* **2004**, *52*, 1−681.

Scheme 1

electron configuration and two S,S-coordinated, closed-shell benzene-1,2-dithiolate(2−) or, alternatively, two 1,2-disubstituted ethylene-1,2-dithiolate(2−) ligands (Scheme 1). Recently, Garner et al.[2] have reported a series of such structurally characterized complexes containing two asymmetric dithiolato ligands.

It has been discovered electrochemically that these monoanions represent the central member of an electron-transfer series $[Au(L)_2]^z$ ($z = 2-$, $1-$, 0).[3] A neutral complex has been structurally characterized, $[Au^{III}(bdt^\bullet)(bdt)] \leftrightarrow [Au^{III}(bdt)(bdt^\bullet)]$, where $(bdt^\bullet)^{1-}$ represents the π radical monoanion of benzene-1,2-dithiolate, $(bdt)^{2-}$.[4] For this and the corresponding 3,4-di-*tert*-butylbenzene-1,2-dithiolate, $(L^{Bu\bullet})^{1-}$, containing neutral complex,[5] an electronic structure has been elucidated where a central, diamagnetic Au(III) ion is coordinated to a π radical monoanion and a closed-shell dianion. The ligand mixed valency had been clearly established as being delocalized (class III). The latter species is paramagnetic ($S_t = 1/2$ ground state), and its EPR spectrum has been reported.[5] We report here the EPR spectrum of $[Au^{III}(mnt^\bullet)(mnt)]^0 \leftrightarrow [Au^{III}(mnt)(mnt^\bullet)]^0$, where $(mnt)^{2-}$ represents maleonitriledithiolate(2−), and $(mnt^\bullet)^{1-}$ is its π radical anion. For the neutral benzene-1,2-dithiolate species $[Au^{III}(L^{Bu\bullet})(L^{Bu})]$, no resolved ^{197}Au hyperfine coupling has been reported,[5] indicating a small Au character of the SOMO.

In a few instances, the paramagnetic dianion $[Au^{II}(L)_2]^{2-}$ ($S_t = 1/2$) has been investigated by EPR spectroscopy, and it

has been concluded that the SOMO possesses ∼10% Au character in agreement with relatively large ^{197}Au hyperfine coupling constants (Au^{II} character).[6,7]

We present here a new electron-transfer series, which involves the new, bulky dithiolene ligand 1,2-di(4-*tert*-butylphenyl)ethylene-1,2-dithiolene (^{2}LH$_2$):[8] $[Au(^2L)_2]^z$ ($z = 1+$, 0, $1-$, $2-$) (Scheme 1). For the first time, a monocationic species has been isolated and characterized, $[Au^{III}(^3L^\bullet)_2](BF_4)$ (**3**), where $(^3L)^{2-}$ represents the dianion 1,2-di-(4-diphenyl)ethylene-1,2-dithiolate(2−), and $(^3L^\bullet)^{1-}$ is its π radical monoanion. In light of the recent previous work,[5] we anticipated an electronic structure for this species that involves a diamagnetic Au(III) central ion and two antiferromagnetically coupled π radical ligand monoanions yielding an $S_t = 0$ ground state: $[Au(^3L^\bullet)_2]^+$. For comparison, we have also prepared the isoelectronic, diamagnetic, but neutral complex $[Pd^{II}(^2L^\bullet)_2]$ (**4**) and structurally characterized it.

We report the experimentally established electronic structures of each member of the electron-transfer series $[Au(L)_2]^z$ ($z = 1+$, 0, $1-$, $2-$) and show that dithiolene ligands exist as closed-shell diamagnetic dianions, $(L)^{2-}$, or as their one-electron oxidized π radical monoanion, $(L^\bullet)^{1-}$, in such complexes.

We have also performed DFT calculations on each member of the series, which establish unequivocally that the diamagnetic monocation $[Au^{III}(^1L^\bullet)_2]^+$ is a singlet diradical. $(^1L)^{2-}$ represents the dianion 1,2-di(phenyl)ethylene-1,2-dithiolate, and $(^1L^\bullet)^{1-}$ is its π radical monoanion. Time-dependent DFT calculations have allowed the assignment of transitions in the electronic spectra in the near-infrared region as an intervalence charge transfer (IVCT) band in $[Au^{III}(^1L^\bullet)(^1L)] \leftrightarrow [Au^{III}(^1L)(^1L^\bullet)]$ and a ligand-to-ligand CT band (LLCT) in $[Au(^1L^\bullet)_2]^+$. The EPR spectral parameters of the neutral and dianionic species have also been calculated.

Experimental Section

The complex $[N(n\text{-Bu})_4][Au^{III}(mnt)_2]$ was prepared as described in the literature.[9a] Reflux of 4,4′-di-*tert*-butylbenzoin with P$_4$S$_{10}$ in 1,4-dioxane affords the ligand 1,2-di-(4-*tert*-butylphenyl)-ethylene-1,2-dithiolene, (^{2}LH$_2$), in situ according to refs 8 and 9b. The same procedure has been used for the synthesis of 1,2-di(4-diphenyl)-ethylene-1,2-dithiol, (^{3}LH$_2$).

$[N(n\text{-Bu})_4][Au(^2L)_2]\cdot 2.25$ CH$_2$Cl$_2$ (1). To a solution of 1,4-dioxane (5 mL) and 4,4′-di-*tert*-butylbenzoin (0.41 g; 1.25 mmol) was added P$_4$S$_{10}$ (0.4 g; 0.91 mmol). After the solution was heated to reflux for 2.5 h in the presence of air, the solution was cooled to 20 °C, and an excess of P$_4$S$_{10}$ was removed by filtration. To the resulting yellow solution was added an aqueous solution (1 mL) of Na[AuCl$_4$]·2H$_2$O (0.22 g; 0.56 mmol). The mixture was heated to reflux for 1 h, after which time a green-brown precipitate was removed from the green solution by filtration. The solution was

(2) Tunney, J. M.; Blake, A. J.; Davies, E. S.; McMaster, J.; Wilson, C.; Garner, C. D. *Polyhedron* **2006**, *25*, 591.

(3) (a) Wang, K. *Progr. Inorg. Chem.* **2006**, *52*, 267 and references therein. (b) Balch, A. L.; Dance, I. G.; Holm, R. M. *J. Am. Chem. Soc.* **1968**, *90*, 1139. (c) Schiødt, N. C.; Sommer-Larsen, P.; Bjørnholm, T.; Folmer Nielsen, M.; Larsen, J.; Bechgaard, K. *Inorg. Chem.* **1995**, *34*, 3688. (d) Nakamoto, M. *Kagaku to Kogyo (Osaka)* **1994**, *68*, 463.

(4) Rindorf, G.; Thorup, N.; Bjørnholm, T.; Bechgaard, K. *Acta Crystallogr., Sect. C* **1990**, *C46*, 1437.

(5) Ray, K.; Wehyermüller, T.; Goosens, A.; Crajé, M. W. J.; Wieghardt, K. *Inorg. Chem.* **2003**, *42*, 4082.

(6) Schlupp, R. L.; Maki, A. H. *Inorg. Chem.* **1974**, *13*, 44.

(7) (a) Van Rens, J. G. M.; Viegers, M. P. A.; de Boer, E. *Chem. Phys. Lett.* **1974**, *28*, 104. (b) Ihlo, L.; Stösser, R.; Hofbauer, W.; Böttcher, R.; Kirmse, R. *Z. Naturforsch.* **1999**, *54b*, 597.

(8) Patra, A. K.; Bill, E.; Weyhermüller, T.; Stobie, K.; Bell, Z.; Ward, M. D.; McCleverty, J. A.; Wieghardt, K. *Inorg. Chem.* **2006**, *45*, 6541.

(9) (a) Waters, J. H.; Gray, H. B. *J. Am. Chem. Soc.* **1965**, *87*, 3534. (b) Schrauzer, G. N.; Mayweg, V. P.; Heinrich, W. *Inorg. Chem.* **1965**, *4*, 1615. (c) Schrauzer, G. N.; Mayweg, V. P. *J. Am. Chem. Soc.* **1965**, *87*, 1483.

then layered with 3 mL of an ethanolic solution of [N(*n*-Bu)$_4$]Br (0.19 g; 0.56 mmol). Within 24 h at 20 °C a microcrystalline, yellow precipitate was obtained, which was filtered off and washed with *n*-hexane. Recrystallization from a CH$_2$Cl$_2$/*n*-hexane (1:1 v/v) mixture afforded yellow crystals suitable for X-ray crystallography. Yield: 80 mg (13%). ESI mass spectrum: pos. ions *m/z* = 242 (100%) [N(*n*-Bu)$_4$]$^+$; neg. ion *m/z* = 905 (100%) [Au(^{2}L)$_2$]$^-$. Anal. Calcd for C$_{60}$H$_{88}$NS$_4$Au: C, 63.52; H, 8.78; N, 1.23; S, 11.30; Au, 17.36. Found: C, 63.7; H, 8.5; N, 0.9; S, 10.7; Au, 16.9.

[Au(^{2}L)(^{2}L$^•$)]·CH$_2$Cl$_2$ (2). To a degassed solution of **1** (35 mg; 0.03 mmol) in CH$_2$Cl$_2$ (5 mL) was added ferrocenium hexafluorophosphate, [Fc]PF$_6$ (11 mg; 0.03 mmol), under an Ar blanketing atmosphere. The mixture was stirred at 20 °C for 2 h, after which time a green solution was obtained. Green microcrystals precipitated upon layering of the solution with dry methanol. Yield: 21 mg. Anal. Calcd for C$_{44}$H$_{52}$S$_4$Au: C, 58.32; H, 5.78; S, 14.15; Au, 21.74. Found: C, 58.1; H, 5.7; S, 14.0; Au, 21.6.

[Au(^{3}L$^•$)$_2$](BF$_4$) (3). The synthesis of [N(*n*-Bu)$_4$][Au^{III}(^{3}L)$_2$] has been executed in a fashion analogous to that described above for **1** by using 4,4′-diphenylbenzoin as starting material. The compound has not been characterized in detail but was used for the following oxidation reaction. To a degassed, dry solution of [N(*n*-Bu)$_4$][Au^{III}-(^{3}L)$_2$] (30 mg; 0.024 mmol) in CH$_2$Cl$_2$ (4 mL) was added [NO]-BF$_4$ (8 mg; 0.07 mmol) under an Ar blanketing atmosphere. The mixture was stirred at 20 °C for 1.5 h, yielding a dark green solution from which upon layering with *n*-hexane a green precipitate was obtained. Yield: 0.01 g (40%). ESI-mass spectrum: pos. ion mode *m/z* = 985 {Au(^{3}L)$_2$}$^+$; negative ion mode *m/z* = 87 [BF$_4$]$^-$. Anal. Calcd for C$_{52}$H$_{36}$S$_4$AuBF$_4$: C, 58.21; H, 3.38; S, 11.96. Found: C, 58.4; H, 3.3; S, 11.8.

[Pd(^{2}L$^•$)$_2$] (4). 4,4′-*tert*-Butylbenzoin (1.37 g; 4 mmol) was refluxed for 3 h with 1.25 g (2.82 mmol) of P$_4$S$_{10}$ in 8 mL of xylene. PdCl$_2$ (0.176 g; 1 mmol) suspended in 20 mL of a methanol/water mixture (10:1) was added to the cooled and filtered solution. After 8 h of stirring at room temperature, the precipitated brown powder was filtered off and washed with methanol. Yield: 0.38 g (47%). Anal. Calcd for C$_{44}$H$_{52}$S$_4$Pd: C, 64.80; H, 6.43. Found: C, 64.85; H, 6.58. ESI mass spectrum (CH$_2$Cl$_2$ solution): *m/z* = 814.4 [Pd-(L)$_2$]$^+$. Single crystals of [Pd(L)$_2$]·0.5toluene suitable for X-ray crystallography were grown from a toluene solution by slow evaporation of the solvent.

X-ray Crystallographic Data Collection and Refinement of the Structures. A yellow single crystal of **1**·2.25CH$_2$Cl$_2$, brown crystals of **2**·CH$_2$Cl$_2$, and **4**·0.5toluene were coated with perfluoropolyether and picked up with a glass fiber. The crystals were immediately mounted in the nitrogen cold stream (100 K) of a Nonius Kappa-CCD diffractometer equipped with a Mo-target rotating-anode X-ray source and a graphite monochromator (Mo Kα, λ = 0.71073 Å). Final cell constants were obtained from least-squares fits of all measured reflections. Crystallographic data of the compounds are listed in Table 1. The Siemens ShelXTL[10] software package was used for solution and artwork of the structure, and ShelXL97[11] was used for the refinement. The structures were readily solved by direct and Patterson methods and subsequent difference Fourier techniques. All non-hydrogen atoms in **1** and **4** were refined anisotropically. The crystals of **2** were extremely small, and, due to a poor data−parameter ratio, only gold, sulfur, and chlorine atoms were anisotropically refined. Hydrogen atoms were placed at calculated positions and refined as riding atoms with isotropic displacement parameters. The asymmetric unit in **1**

Table 1. Crystallographic Data for **1**·2.25CH$_2$Cl$_2$, **2**·CH$_2$Cl$_2$, **4**·0.5Toluene

	1·2.25CH$_2$Cl$_2$	**2**·CH$_2$Cl$_2$	**4**·0.5toluene
chem formula	C$_{62.25}$H$_{92.5}$AuCl$_{4.5}$NS$_4$	C$_{45}$H$_{54}$AuCl$_2$S$_4$	C$_{47.5}$H$_{56}$PdS$_4$
fw	1339.60	990.99	861.56
space group	*P*-1, No. 2	*P*4$_1$2$_1$2, No. 92	*Pna*2$_1$, No. 33
a, Å	17.7270(4)	11.705(1)	11.9728(5)
b, Å	17.8283(4)	11.705(1)	35.8262(14)
c, Å	24.6899(6)	64.778(5)	11.1766(4)
α, deg	69.394(5)	90	90
β, deg	89.774(5)	90	90
γ, deg	65.875(5)	90	90
V, Å	6575.9(3)	8875.0(13)	4794.1(3)
Z	4	8	4
T, K	100(2)	100(2)	100(2)
ρ calcd, g cm^{-3}	1.353	1.483	1.194
refln collected/2θ$_{max}$	181 310/70.0	17 723/45.0	25 566/52.0
unique refln/*I* > 2σ(*I*)	57 536/50 115	4515/2630	8749/7571
no. of params/restr.	1405/77	254/7	503/1
μ, cm^{-1}/λ, Å	25.84/0.71073	14.83/0.71073	5.90/0.71073
R1[a]/GOF[b]	0.0338/1.033	0.0746/1.029	0.0395/1.041
wR2[c] (*I* > 2σ(*I*))	0.0784	0.0971	0.0804
residual density, e Å^{-3}	+3.18/−2.69	+0.86/−1.04	+0.59/−0.64

[a] Observation criterion: $I > 2\sigma(I)$. R1 $= \sum ||F_o| - |F_c||/\sum|F_o|$. [b] GOF $= [\sum[w(F_o^2 - F_c^2)^2]/(n - p)]^{1/2}$. [c] wR2 $= [\sum[w(F_o^2 - F_c^2)^2]/\sum[w(F_o^2)^2]]^{1/2}$, where $w = 1/\sigma^2(F_o^2) + (aP)^2 + bP$, $P = (F_o^2 + 2F_c^2)/3$.

contains three crystallographically independent complex anions of which two reside on a center of inversion, two NBu$_4$ cations and 4.5 dichloromethane solvent molecules. One of the NBu$_4$ cations in **1** was found to be disordered and was split on two positions in a ratio of about 83:17. Two tertiary butyl groups attached to C(42) and C(66) were also split in ratios of 57:43 and 59:41, respectively. The dichloromethane molecule containing C(900) was given an occupation factor of 0.5 because it is found to be disordered next to a crystallographic inversion center. Geometries of the split models were restrained using EADP, SAME, and SADI instructions of ShelXL97[11] (77 restraints). The dichloromethane molecule in **2** is disordered and was split in a ratio of 59:41. Displacement parameters and C−Cl and Cl−Cl distances were restrained to be equal. The toluene solvent molecule in crystals of **4** was not fully occupied, and an occupation factor of 0.5 was used.

Calculations. All calculations in this work were performed with the electronic structure program ORCA.[12] The geometry optimizations were carried out at the BP86 level of DFT.[13] Because this work is concerned with heavy transition metal complexes of Au and Pd, scalar relativistic corrections were included using the second-order Douglas−Kroll−Hess (DKH2)[14] and zeroth-order regular approximation (ZORA)[15a] method.

In the geometry optimizations, the one-center approximation was used, which eliminates DKH2 contributions to the analytic gradients. In the context of the ZORA approximation, it was shown that the one-center approximation only introduces minor errors into a final geometries.[15b] Large uncontracted Gaussian basis sets were used at the metal center, which were derived from the well-tempered basis sets of Huzinaga.[16] For the remaining atoms, the all-electron polarized triple-ξ (TZVP)[17] Gaussian basis sets of the Ahlrichs

(10) *ShelXTL*, V.5; Siemens Analytical X-Ray Instruments, Inc., 1994.

(11) Sheldrick, G. M. *ShelXL97*; Universität Göttingen, 1997.

(12) Neese, F. *ORCA an Ab Initio, Density Functional and Semiempirical Electronic Structure Program Package*, Version 2.4, revision 36; Max-Planck-Institut für Bioanorganische Chemie: Mülheim/Ruhr, Germany, May 2005.

(13) (a) Becke, A. D. *J. Chem. Phys.* **1988**, *84*, 4524. (b) Perdew, J. P. *Phys. Rev. B* **1986**, *33*, 8522.

(14) Hess, B. A.; Marian, C. M. In *Computational Molecular Spectroscopy*; Jensen, P., Bunker, P. R., Eds.; John Wiley & Sons: New York, 2000; p 169 ff.

(15) (a) van Lenthe, E.; Snijders, J. G.; Baerends, E. J. *J. Chem. Phys.* **1996**, *105*, 6505. (b) van Lenthe, E.; Faas, S.; Snijders, J. G. *Chem. Phys. Lett.* **2000**, *328*, 107.
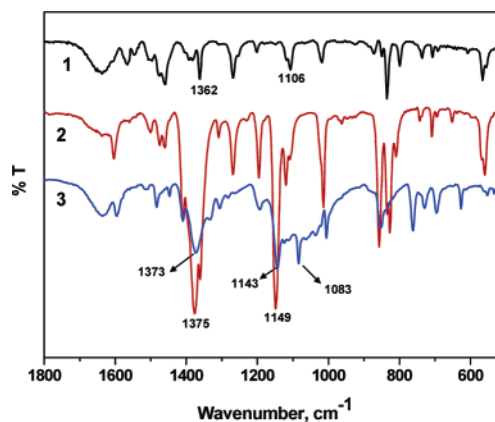
group were used in an uncontracted form to allow for a distortion of the inner shell orbitals in the presence of the relativistic potential. All calculated structures were verified to represent local minima by calculation of harmonic frequencies. No negative frequencies were observed. The $\langle s^2 \rangle$ expectation value for $[\text{Au}(^1\text{L})(^1\text{L}^\bullet)]^0$ is 0.75118, and for $[\text{Au}(^1\text{L})_2]^{2-}$ it is 0.75152.

The property calculations at the optimized geometries were done with the B3LYP functional.[18] In this case, the same basis sets were used, but the scalar-relativistic ZORA method was used because in this formalism magnetic properties are more readily formulated.[19a] For the ZORA calculations, the method of van Wüllen[19b] is implemented in ORCA. Care was taken to ensure accurate numerical integration in the presence of steep basis functions. Details of the methods used to calculate the *g*-tensor and metal hyperfine couplings can be found in ref 20a–c. Because the recently implemented SOMF (spin orbit mean-field) orperator[20c] is presently only available in the Breit–Pauli version, which is known to be unsatisfactory for heavy elements, we have resorted to the effective charge SOC (spin orbit coupling) Hamiltonian of Koseki et al.[20d,e] However, because we have performed all-electron calculations using scalar relativistic corrections, the effective nuclear charges for Pd and Au needed to be adjusted. From comparison between calculated SOC matrix elements with effective one-electron SOC constants, the values $Z_{\text{eff}}(\text{Pd}) = 14.3$ and $Z_{\text{eff}}(\text{Au}) = 27.5$ were determined, which lead to ξ_{nd} values of ~ 1300 cm^{-1} (Pd) and ~ 4500 cm^{-1} (Au), respectively. All other effective nuclear charges had their default values. TD-DFT calculations were carried out according to ref 20f. Natural population analysis (NPA)[21a–c] was done through an interface of ORCA to the Gennbo program version 5.0.[21d] Isocontour plots were done with the ChemBats3D program.[22]

Physical Measurements. Electronic spectra of complexes in CH$_2$Cl$_2$ solution were recorded at Mülheim on a scanning double beam UV–vis–NIR spectrophotometer (Perkin-Elmer, Lambda 19) in the range 200–2000 nm, and at Vermont on an Olis Cary-14 spectrometer. Cyclic voltammograms and coulometric measurements were performed by using an EG&G potentiostat/galvanostat (model 273A). X-band EPR spectra at Mülheim were recorded on a Bruker ELEXSYS E500 spectrometer equipped with a He flow cryostat (Oxford Instruments ESR 910) and Hewlett-Packard frequency counter HP 5253B. Those recorded at Vermont were obtained with a Bruker 300E instrument. The spectra were simulated on the basis of a spin-Hamiltonian description of the electronic ground state with $S = \frac{1}{2}$:

$$\hat{H} = \mu_\text{B} \vec{B} \cdot g \cdot \hat{\vec{S}} - g_\text{N} \mu_\text{N} \vec{B} \cdot \hat{\vec{I}} + \hat{\vec{S}} \cdot A \cdot \hat{\vec{I}} + \hat{\vec{I}} \cdot P \cdot \hat{\vec{I}}$$

by using the simulation package XSOPHE.[23]

(16) (a) Huzinaga, S.; Miguel, B. *Chem. Phys. Lett.* **1990**, *175*, 289. (b) Huzinaga, S.; Klobukowski, M. *Chem. Phys. Lett.* **1993**, *212*, 260.
(17) (a) Schäfer, A.; Horn, H.; Ahlrichs, R. *J. Chem. Phys.* **1992**, *97*, 2571. (b) Schäfer, A.; Huber, C.; Ahlrichs, R. *J. Chem. Phys.* **1994**, *100*, 5289. (c) Ahlrichs, R.; May, K. *Phys. Chem. Chem. Phys.* **2000**, *2*, 943–945.
(18) (a) Lee, C.; Yang, W.; Parr, R. G. *Phys. Rev. B* **1988**, *37*, 785. (b) Becke, A. D. *J. Chem. Phys.* **1993**, *98*, 5648.
(19) (a) van Lenthe, E.; van der Avoird, A.; Wormer, P. E. S. *J. Chem. Phys.* **1998**, *108*, 4783. (b) van Wüllen, C. *J. Chem. Phys.* **1998**, *109*, 392.
(20) (a) Neese, F. *J. Chem. Phys.* **2001**, *115*, 11080. (b) Neese, F. *J. Chem. Phys.* **2003**, *118*, 3939. (c) Neese, F. *J. Chem. Phys.* **2005**, *122*, 034107. (d) Koseki, S.; Gordon, M. S.; Schmidt, M. W.; Matsunaga, N. *J. Phys. Chem.* **1995**, *99*, 12764. (e) Koseki, S.; Schmidt, M. W.; Gordon, M. S. *J. Phys. Chem. A* **1998**, *102*, 10430. (f) Neese, F.; Olbrich, G. *Chem. Phys. Lett.* **2002**, *362*, 170.

Figure 1. Infrared spectra of solid **1** (in black), **2** (in red), and **3** (in blue) in the range 500–1800 cm^{-1} (KBr disks).

Results and Discussion

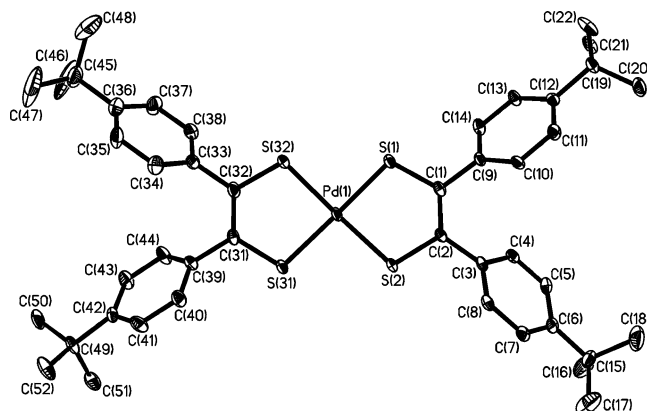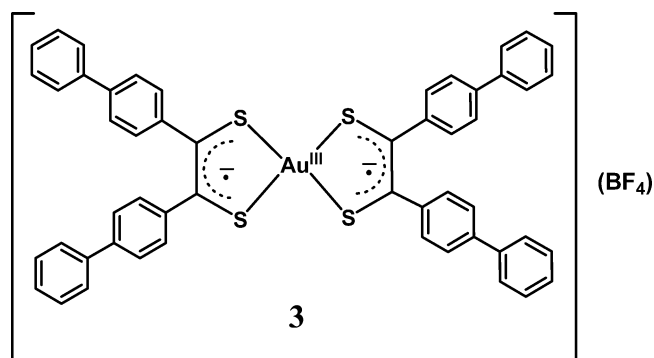**Syntheses and Crystal Structures.** Upon heating a 1,4-dioxane solution of 4,4′-di-*tert*-butylbenzoin or 4,4′-diphenylbenzoin and P$_4$S$_{10}$ for 3 h to reflux, the ligand 1,2-di(4-*tert*-butylphenyl)ethylene-1,2-dithiolene, ^{2}LH$_2$, or ^{3}LH$_2$ was generated in situ.[8,9] The addition of Na[AuCl$_4$]·2H$_2$O and [N(*n*-Bu)$_4$]Br and heating to reflux initiated the precipitation of yellow, diamagnetic crystals of [N(*n*-Bu)$_4$][Au(^{2}L)$_2$] (**1**). If PdCl$_2$ was used as a starting material, the blue neutral complex [Pd(^{2}L$^\bullet$)$_2$] (**4**) was obtained in crystalline form. Complex **4** was also diamagnetic as was judged from its ^{1}H NMR spectrum.

The reaction of **1** with 1 equiv of ferrocenium hexafluorophosphate in CH$_2$Cl$_2$ yielded green crystals of [Au(^{2}L)(^{2}L$^\bullet$)]·CH$_2$Cl$_2$ (**2**). This complex is paramagnetic. Temperature-dependent (4–300 K) magnetic susceptibility measurements in an 1.0 T magnetic field on a solid sample of **2** revealed a temperature-independent (50–300 K) magnetic moment of 1.72 μ_B, indicating an $S = \frac{1}{2}$ ground state for **2**.

Figure 1 displays the infrared spectra of **1**, **2**, and **3** (KBr disks) in the range 500–1800 cm^{-1}. The spectra of **1** and **2** exhibit many features in common. Notable differences include very strong bands at 1375, 1149, and 857 cm^{-1} in the spectrum of **2**. The bands at 1149 and 1143 cm^{-1} are unique in the spectra of **2** and **3**, respectively; it is assigned to a predominantly $\nu(\text{C}{=}\text{S}^\bullet)$ stretching mode.[1,5] This mode is indicative of the presence of a coordinated π radical monoanion (L$^\bullet$)$^{1-}$; it has also been identified for monoanionic, S,S-coordinated 3,5-di-*tert*-butyl-benzene-1,2-dithiolate(1−) π radicals.[5,24,25] It has previously been observed for [Au$^{\text{III}}$(L$^{\text{Bu}}$)(L$^{\text{Bu}\bullet}$)] ↔ [Au$^{\text{III}}$(L$^{\text{Bu}\bullet}$)(L$^{\text{Bu}}$)] at 1085 cm^{-1}. The

(21) (a) Reed, A. E.; Weinhold, F. *J. Chem. Phys.* **1983**, *78*, 4066. (b) Reed, A. E.; Weinstock, R. B.; Weinhold, F. *J. Chem. Phys.* **1985**, *83*, 735. (c) Reed, A. E.; Curtiss, L. A.; Weinhold, F. *Chem. Rev.* **1988**, *88*, 899. (d) Glendening, E. D.; Badenhoop, J. K.; Reed, A. E.; Carpenter, J. E.; Bohmann, J. A.; Morales, C. M.; Weinhold F. *NBO 5.0*; Theoretical Chemistry Institute, University of Wisconsin: Madison, WI, 2001; http://www.chem.wisc.edu/~nbo5.
(22) *Chem.Bats3d*, version 6.0; CambridgeSoft.com, 2000.
(23) Hanson, G. R.; Gates, K. E.; Noble, C. J.; Griffin, M.; Mitchell, A.; Benson, S. *J. Inorg. Biochem.* **2004**, *98*, 903.
(24) Ray, K.; Weyhermüller, T.; Neese, F.; Wieghardt, K. *Inorg. Chem.* **2005**, *44*, 5345.
(25) Petrenko, T.; Ray, K.; Wieghardt, K.; Neese, F. *J. Am. Chem. Soc.* **2006**, *128*, 4422.
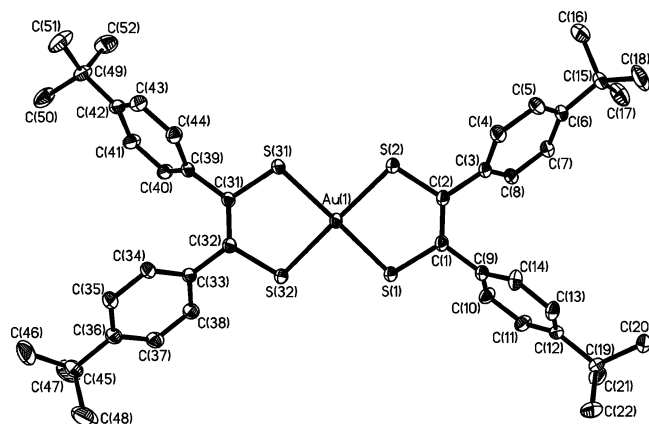
Figure 2. Structure of the anion $[Au^{III}(^2L)_2]^-$ in crystals of **1**. The structure of the neutral species $[Au^{III}(^2L)(^2L^\bullet)] \leftrightarrow [Au^{III}(^2L^\bullet)(^2L)]$ in crystals of **2** is similar and not shown.

Figure 3. Structure of the neutral $[Pd^{II}(^2L^\bullet)_2]$ molecule in crystals of **4**.

Scheme 2
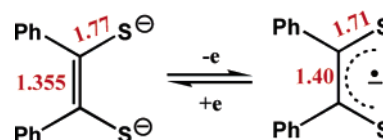
Table 2. Selected Average Bond Distances and Standard Deviations in **1**, **2**, and **4** in angstroms

	complex		
	1	**2**	**4**
M–S	2.3148(5)	2.291(5)	2.251(1)
C–S	1.769(2)	1.749(20)	1.708(4)
C_1–C_2	1.355(3)	1.36(2)	1.399(5)

IR spectrum of **4** displays this $\nu(C{=}S^\bullet)$ band also at 1149 cm^{-1}; for $[Pd(S_2C_2Ph_2)_2]$, it has been observed at 1136 cm^{-1}.[9c]

When the above oxidation reaction was carried out on $[N(n\text{-}Bu)_4][Au^{III}(^3L)_2]$ in CH_2Cl_2 solution with 2–3 equiv of $[NO]BF_4$, a dark green solution was obtained from which upon layering with *n*-hexane a dark green precipitate of $[Au^{III}(^3L^\bullet)_2](BF_4)$ (**3**) was obtained in 40% yield. Complex **3** is diamagnetic and displays an intense $\nu(C{=}S^\bullet)$ stretching mode at 1149 cm^{-1} (Figure 1), which is absent in the IR spectrum of $[N(n\text{-}Bu)_4][Au^{III}(^3L)_2]$. The electronic spectrum of **3** recorded in CH_2Cl_2 displays the same set of absorption maxima as that of electrochemically generated $[Au^{III}(^2L^\bullet)_2]^+$ (see below and Table 3).
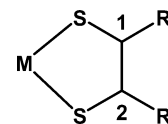

Figure 2 shows the structure of the monoanion $[Au^{III}(^2L)_2]^-$ in crystals of **1**; that of the neutral molecule $[Au^{III}(^2L^\bullet)(^2L)]$ $\leftrightarrow [Au^{III}(^2L)(^2L^\bullet)]^-$ in crystals of **2** is similar and not shown. We note that the quality of the crystal structure determination of neutral **2** is below standards. The estimated standard deviations (esd) are too large to allow a discussion of C–C and C–S bond lengths, but the atom connectivity and square-planar coordination geometry is unequivocally established. Table 2 summarizes important bond lengths and angles in **1** and **2**. The structure of the neutral molecule $[Pd^{II}(^2L^\bullet)_2]$ in crystals of **4** is shown in Figure 3; selected bond lengths are again listed in Table 2.

It is noteworthy that the average Au–S bond lengths in **1** at 2.315 ± 0.002 Å and in **2** at 2.291 ± 0.015 Å are very similar indeed. This observation together with the calcula-

tions discussed below show that one-electron oxidation of **1** to **2** does not involve the central Au^{III} ion (no Au^{IV} in **2**). On the other hand, the av C–S bond distance in **1** at 1.769 ± 0.006 Å is long and indicates a closed-shell dianion $(^2L)^{2-}$, whereas in **4** it is short at 1.708 ± 0.01 Å. A straightforward explanation of this trend is as follows: in **1** there are an Au^{III} center and two closed-shell dithiolato(2–) ligands present.[24] The observed long C–S distance is in excellent agreement with a number of structures containing bis-(dithiolato)gold(III) monoanions reported recently by Garner et al.[2] In **4**, there are a Pd^{II} central ion and two monoanionic π radical ligands present with a short av C–S bond at 1.71 ± 0.01 Å. Scheme 2 summarizes the important C–S and olefinic C–C bond distances in the closed-shell dianionic form $(^1L)^{2-}$ and its π radical monoanion $(^1L^\bullet)^{1-}$ as was determined by X-ray crystallography.[26] In excellent agreement with the above model is the behavior found for the olefinic C–C bond distances in **1** and **4**. In **1**, this bond length is at an av of 1.35 ± 0.01 Å; it has considerable double bond character. In contrast, this bond in **4** is found at an av 1.40 ± 0.01 Å, which is significantly longer than in **1**. The C–C bonds in **2** cannot be discussed due to the low X-ray

(26) $[Pt(^1L^\bullet)_2]$: Dessy, G.; Fares, V.; Bellito, C.; Flamini. *Cryst. Struct. Commun.* **1982**, *11*, 1743. $[Ni(^1L^\bullet)_2]$: Kuramoto, N.; Asao, K. *Dyes Pigm.* **1990**, *12*, 65. $[Ni(^1L^\bullet)_2]$: Megnamisi-Belombe, M.; Nuber, B. *Bull. Chem. Soc. Jpn.* **1989**, *62*, 4092.
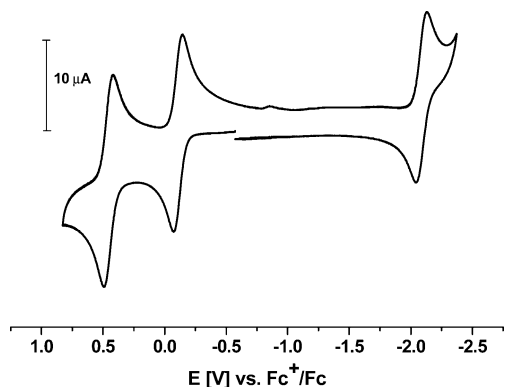
Figure 4. Cyclic voltammogram of **1** in CH_2Cl_2 solution (0.10 M [N(*n*-Bu)$_4$]PF$_6$) at 25 °C at a scan rate of 200 mV s^{-1} (conditions: glassy carbon working electrode; ferrocene (Fc) internal standard).
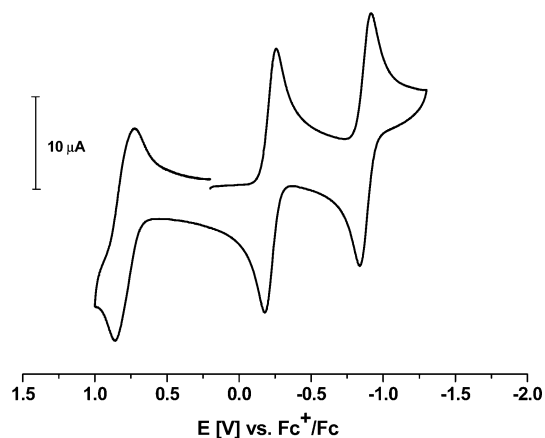
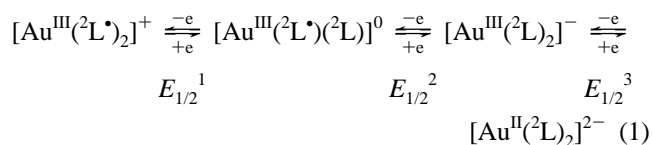**Figure 5.** Cyclic voltammogram of **4** in CH_2Cl_2 solution (0.10 M [N(*n*-Bu)$_4$]PF$_6$) at 25 °C at a scan rate of 400 mV s^{-1} (conditions: glassy carbon working electrode; ferrocene internal standard).

quality of the crystals and, consequently, the large error of ± 0.1 Å. In Garner's complexes in ref 2, the av C−C distance is reported at 1.34 ± 0.01 Å corresponding to an [Au^{III}(L)$_2$]$^-$ electronic structure with two dithiolato(2−) ligands.

Electrochemistry. Cyclic voltammograms (cv) of **1** and **4** have been recorded in CH_2Cl_2 solutions containing 0.10 M [(*n*-Bu)$_4$]PF$_6$ supporting electrolyte at 20 °C at a glassy carbon working electrode. All potentials are referenced versus the ferrocenium/ferrocene (Fc$^+$/Fc) couple. The cv of **1** is shown in Figure 4, and that of **2** is identical to that of **1**.

Three fully reversible one-electron-transfer waves have been observed at $E_{1/2}^1 = +0.45$ V, $E_{1/2}^2 = -0.11$ V, and $E_{1/2}^3 = -2.09$ V in the cv of **1** and **2**. Controlled potential coulometric measurements established that monoanionic **1** undergoes two successive one-electron oxidations and a one-electron reduction at a very negative potential, eq 1.
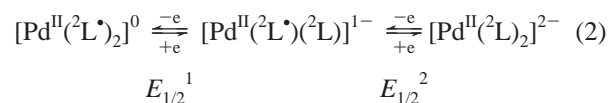
$$[\text{Au}^{III}(^2\text{L}^\bullet)_2]^+ \underset{+e}{\overset{-e}{\rightleftharpoons}} [\text{Au}^{III}(^2\text{L}^\bullet)(^2\text{L})]^0 \underset{+e}{\overset{-e}{\rightleftharpoons}} [\text{Au}^{III}(^2\text{L})_2]^- \underset{+e}{\overset{-e}{\rightleftharpoons}}$$

$$E_{1/2}^1 \qquad\qquad E_{1/2}^2 \qquad\qquad E_{1/2}^3$$

$$[\text{Au}^{II}(^2\text{L})_2]^{2-} \quad (1)$$

The cv of **3** displays the same three redox waves at $E_{1/2}^1 = +0.51$ V, $E_{1/2}^2 = -0.07$ V, and $E_{1/2}^3 = -2.03$ V. The cv of **4** is displayed in Figure 5. Interestingly, only two reversible electron-transfer waves are observed at $E_{1/2}^1 = -0.41$ V and
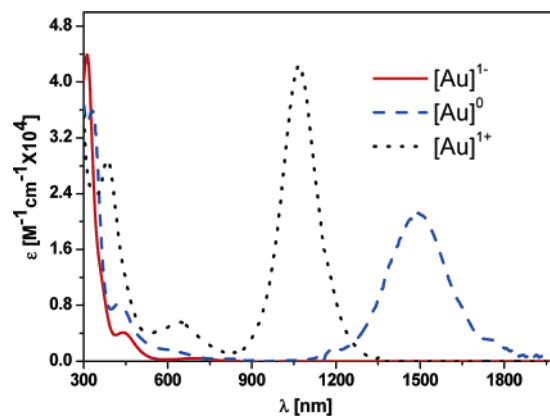
Figure 6. Electronic spectra of **1** (red), and **2** (blue dashed line), and the electrochemically generated monocation [Au^{III}(^{2}L$^\bullet$)$_2$]$^+$ (black dotted line) in CH_2Cl_2 solution (0.2 M [N(*n*-Bu)$_4$]PF$_6$) at −25 °C.

$E_{1/2}^2 = -1.07$ V as indicated in eq 2. Both correspond to successive one-electron reductions generating a mono- and then a dianion, eq 2. A third quasi-reversible (oxidation) wave is observed at $E_{1/2}^0 = +0.60$ V, which may correspond to the [Pd(L)$_2$]$^{1+}$/[Pd(L)$_2$]^0 couple. This process has not been investigated further.

$$[\text{Pd}^{II}(^2\text{L}^\bullet)_2]^0 \underset{+e}{\overset{-e}{\rightleftharpoons}} [\text{Pd}^{II}(^2\text{L}^\bullet)(^2\text{L})]^{1-} \underset{+e}{\overset{-e}{\rightleftharpoons}} [\text{Pd}^{II}(^2\text{L})_2]^{2-} \quad (2)$$

$$E_{1/2}^1 \qquad\qquad E_{1/2}^2$$

The oxidation of [Au(mnt)$_2$]$^-$ was investigated in CH_2Cl_2, using either 0.1 M [NBu$_4$][PF$_6$] or [NBu$_4$][B(C$_6$F$_5$)$_4$] as the supporting electrolyte with identical results. A diffusion-controlled Nernstian-shaped one-electron oxidation was observed ($E_{1/2} = 0.91$ V), the electron-transfer stoichiometry being confirmed by bulk coulometry. As the coulometric oxidation proceeded, the solution turned a dark gray, which is assumed to be the color of neutral [Au(mnt)(mnt$^\bullet$)]. Solutions taken at this point gave optical and EPR spectra consistent with this premise (vide infra). It was noticed that a dark gray precipitate formed after completion of the electrolysis and that this was accelerated at lower temperatures. However, our attempts at isolation of this very fine precipitate resulted only in its spontaneous reduction back to the Au(III) monoanion, [Au(mnt)$_2$]$^-$. It has been noted previously that neutral [M(mnt$^\bullet$)$_2$] complexes (M = Ni group) generally display poor solubilities, because of the likely formation of weakly coordinated oligomers.[27] Slow formation of oligomers would also account for the poor solubility of the corresponding Au complex.

Optical Spectroscopy. Electronic spectra of **1**, **2**, and the electrochemically generated monocation [Au^{III}(^{2}L$^\bullet$)$_2$]$^+$ have been recorded at −25 °C in CH_2Cl_2 solutions. The CH_2Cl_2 solution spectrum of **3** is very similar to that of the aforementioned cation. The spectrum is shown in Figure 6 and summarized in Table 3. The spectrum of **1** displays two weak d−d transitions in the visible; no charge transfer (CT) bands are observed >600 nm in the near-infrared (NIR).

(27) Geiger, W. E.; Barrière, F.; LeSuer, R. J.; Trupia, S. *Inorg. Chem.* **2001**, *40*, 2472.

Table 3. Electronic Spectra of Complexes in CH_2Cl_2 Solution

complex	λ_{max}, nm (10^4 ϵ, M^{-1} cm^{-1})	ref
$[Au^{III}(^2L)_2]^-$	696(0.04), 441(0.4), 331sh	this work
$[Au^{III}(^2L^\bullet)(^2L)]^0$	1495(2.12), 1184(0.2), 426(0.84)	this work
$[Au^{III}(^2L^\bullet)_2]^+$	1066(4.25), 640(0.6), 383sh	this work
$[Au^{III}(^3L^\bullet)_2]^+$	1142(4.2), 687(0.69), 407(3.5)	this work
$[Pd^{II}(^2L^\bullet)_2]^{0\,a}$	915(3.7), 270(6.0)	this work
$[Pd^{II}(^2L^\bullet)(^2L)]^{-\,a}$	1250(1.7), 296(5.5), 265(5.2)	this work
$[Pd^{II}(^2L)_2]^{2-\,a}$	303(4.3), 245(5.3)	this work
$[Au^{III}(L^{Bu})_2]^{-\,b}$	618(0.008), 415(0.02)	5
$[Au^{III}(L^{Bu\bullet})(^1L^{Bu})]^{0\,b}$	1452(2.7), 1023(0.2), 400(0.6)	5
$[Pd(L^{Bu\bullet})_2]^{0\,b}$	850(5.0), 620(0.8), 379(1.2)	24
$[Pd(L^{Bu\bullet})(L^{Bu})]^{1-\,b}$	1140(2.5), 894(0.5), 408(0.1), 340(7.7)	24
$[Pd(L^{Bu})_2]^{2-\,b}$	392(0.6), 350(0.9)	24
$[Au(mnt^\bullet)(mnt)]^0$	490(0.3), 1110($\sim$1.0)	this work

^{a} At -25 °C. ^{b} $(L^{Bu})^{2-}$ and $(L^{Bu\bullet})^{1-}$ are derivatives of 3,5-di-*tert*-butylbenzene-1,2-dithiol, $H_2(L^{Bu})$.
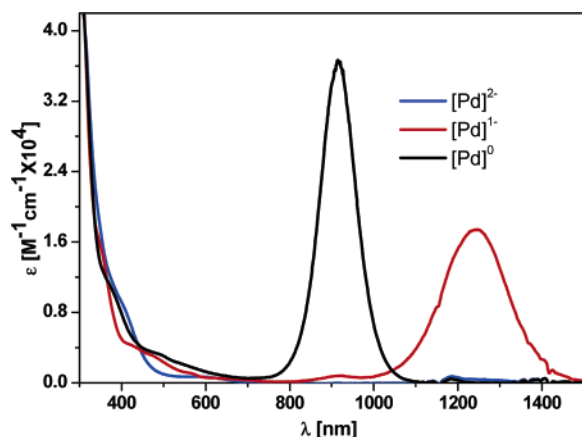
Figure 7. Electronic spectra of neutral **4** (black), the monoanion $[Pd^{II}(^2L^\bullet)(^2L)]^-$ (red), and the dianion $[Pd^{II}(^2L)_2]^{2-}$ (blue), of which the latter two were electrochemically generated in CH_2Cl_2 solution (0.10 M [N(*n*-Bu)_4]PF_6).

Similar spectra have been reported for other diamagnetic, square-planar Au^{III} complexes.

In contrast, the spectrum of **2** displays a very intense absorption maximum in the NIR at 1495 nm ($\epsilon = 2.1 \times 10^4$ M^{-1} cm^{-1}) and a weaker transition at 1184 nm ($\epsilon = 0.2 \times 10^4$ M^{-1} cm^{-1}). These bands have been previously assigned to an intervalence transition of type $[Au^{III}(L^\bullet)(L)] \leftrightarrow [Au^{III}(L)(L^\bullet)]$, which corresponds to a spin allowed transition $1b_{1u} \rightarrow 2b_{2g}$ for $[Au^{III}(L^\bullet)(L)]$ (in D_{2h} symmetry). For the corresponding benzene-1,2-dithiolato complex, this IVCT band has been observed at 1452 nm ($\epsilon = 2.7 \times 10^4$ M^{-1} cm^{-1}).[5] The optical spectrum of $[Au(mnt)(mnt^\bullet)]$ has an intense near-IR absorption at 1110 nm ($\epsilon \approx 10^4$ M^{-1} cm^{-1}).

It is now quite remarkable that the spectra of the monocations $[Au^{III}(^2L^\bullet)_2]^+$ and $[Au^{III}(^3L^\bullet)_2]^+$ display an intense ligand-to-ligand CT in the NIR at both 1066 nm ($\epsilon = 4.2 \times 10^4$ M^{-1} cm^{-1}) and 1142 nm (4.2 $\times 10^4$ M^{-1} cm^{-1}), respectively. This is the first time that this transition has been observed for a gold complex. These LLCT absorption maxima have been reported for neutral bis(benzene-1,2-dithiolate)metal(II) complexes (M = Ni, Pd, Pt).[24] The spectrum of **4** in Figure 7 displays this maximum at 915 nm ($\epsilon = 3.7 \times 10^4$ M^{-1} cm^{-1}), whereas its reduced form $[Pd^{II}(^2L^\bullet)(^2L)]^-$ exhibits this band at 1250 nm ($\epsilon = 1.7 \times 10^4$ M^{-1} cm^{-1}). It has been noted previously[24] that the
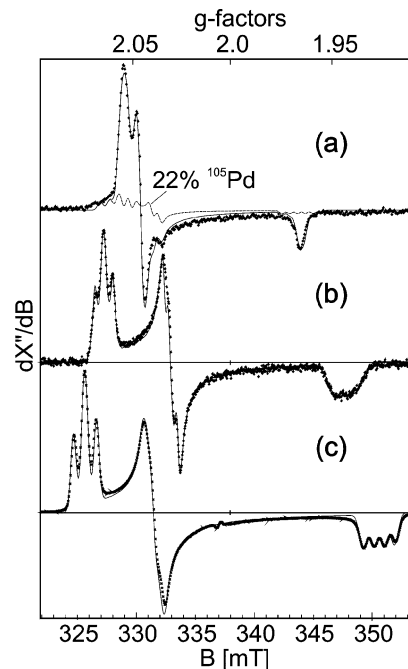
Figure 8. X-band EPR spectra of (a) $[Pd(^2L^\bullet)(^2L)]^-$, (b) $[Au^{III}(^2L^\bullet)(^2L)]^0$, and (c) $[Au^{III}(mnt)(mnt^\bullet)]^0$ in frozen CH_2Cl_2 (at 30 K (a), 90 K (b), and 120 K (c)). Experimental conditions: mw-frequency, (a) 9.43219, (b) 9.42972, (c) 9.46025 GHz; mw-power, (a) 100, (b) 4, (c) 2 μW; modulation amplitude, (a) 0.7, (b) 0.2, (c) 0.5 mT. The solid lines represent spin-Hamiltonian simulations using parameters given in Table 4. The line in the spectrum of (a) is the hyperfine split contribution from ^{105}Pd ($I = {}^5/_2$; 22.2% abundance); electric quadrupole interactions were neglected for ^{105}Pd.

intensity of the LLCT maximum of $[M(L^\bullet)_2]^n$ complexes is at higher energy and twice as intense as the IVCT band for the corresponding one-electron reduced form $[M(L^\bullet)(L)]^{n-1}$. As reported above for $[Au^{III}(^2L)_2]^-$, the corresponding complex $[Pd(^2L)_2]^{2-}$ does not exhibit any absorption maxima $>$400 nm.

From the above analysis of the electronic spectra, it appears that the monocationic species $[Au^{III}(^2L^\bullet)_2]^+$ (and $[Au^{III}(^3L^\bullet)_2]^+$) is isostructural and isoelectronic with the neutral complex $[Pd^{II}(^2L^\bullet)_2]$. Similarly, neutral $[Au^{III}(^2L^\bullet)(^2L)]$ and monoanionic $[Pd^{II}(^2L^\bullet)(^2L)]^{1-}$ possess the same electronic structure as do $[Au^{III}(^2L)_2]^-$ and $[Pd^{II}(^2L)_2]^{2-}$.

X-Band EPR Spectroscopy. The cw-X-band EPR spectra of the neutral gold complexes $[Au(^2L^\bullet)(^2L)]$ (**2**) and $[Au(mnt)(mnt^\bullet)]$ in frozen CH_2Cl_2 solution (0.10 M [N(*n*-Bu)_4]-PF_6) display both anisotropic signals around $g \approx 2$ that are typical of an $S = {}^1/_2$ system with rhombic g factors (Figure 8, panels b and c, Table 4).

The spectra show remarkable hyperfine splitting from the ^{197}Au nucleus ($I = {}^3/_2$, 100% abundance), which deviates from the more normal appearance of the most observed multiplets in having unusual spacing and intensity distribution of the hyperfine lines. Similar anomalies have been observed previously for $[Au^{II}(dithio-carbamate)_2]^{28,29}$ and the $[Au(mnt)_2]^{2-}$ dianion.[6,30,32] The unusual features are caused by a sizable electric field gradient (efg) at the ^{197}Au nucleus

(28) Vängard, T.; Akerström, S. *Nature* **1959**, *184*, 183.
(29) Willigen, H. V.; Rens, J. G. M. *Chem. Phys. Lett.* **1968**, *2*, 283.
(30) Rens, J. G. M.; Boers, E. *Mol. Phys.* **1970**, *19*, 745.

Table 4. EPR Parameters of $[Pd(^2L)(^2L^\bullet)]^-$, $[Au(^2L)(^2L^\bullet)]$ (**2**), and $[Au(mnt)(mnt^\bullet)]$

tensor		$[Pd(^2L)(^2L^\bullet)]^{-c}$	$[Au(^2L)(^2L^\bullet)]$ (**2**)	$[Au(mnt)(mnt^\bullet)]$
G	g_x	1.965(1.960)	1.944	1.928
	g_y	2.046(2.041)	2.030	2.039
	g_z	2.066(2.051)	2.065	2.075
$A \times 10^4$, cm^{-1}	A_x	−6.0(5.0)	−6.8	−8.1
	A_y	−6.0(6.6)	−6.7	−7.0
	A_z	−7.6(9.2)	−6.3	−8.1
	$A_0{}^a$	−6.5	−6.6	−7.7
$P \times 10^4$, cm^{-1}	P_x	n.d.	−150	−150
	P_y	n.d.	+50	+50
	P_z	n.d.	+100	+100
T, K^b		30	90	120

^{a} Isotropic value derived from the anisotropic tensor. ^{b} Temperature. ^{c} Values in brackets refer to $[Pd(^1L)(^1L^\bullet)]^-$ from: Bowmaker, G. A.; Boyd, P. D. W.; Campbell, G. K. *Inorg. Chem.* **1983**, *22*, 1208.

and the corresponding strong quadrupole hyperfine interaction with the principal axes pointing in a different direction from those of the *g* matrix or of the magnetic hyperfine tensor. The misorientation of quantization axes induces mixing of hyperfine levels, line shifts, and "forbidden" transitions in the EPR spectra. In the analysis of our spectra of the neutral $[Au(L)(L^\bullet)]$ (**2**) and $[Au(mnt)(mnt^\bullet)]$ complexes, we followed the previous work and simulated the X-band powder spectra by using mixed magnetic and electric hyperfine interactions.
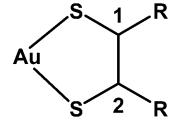
Excellent fits were obtained with the *g*-, *A*-, and *P*-tensor components summarized in Table 4 and shown in Figure 8. Minor details, like small relative rotations of the different tensors principal axes system, could not be resolved, but these are difficult to interpret in quantitative chemical terms anyhow. The signs of the *A*-values also could not be determined from experiment, but were taken from the DFT calculations (see below). However, a comparison of the anisotropic *A* values of $[Au(mnt)(mnt^\bullet)]$ with the result of a measurement performed in liquid solution at 160 K reveals that the three tensor components must have the same sign. This is inferred from the close match of the isotropic value calculated from the anisotropic values given in Table 4 and the value measured at 160 K, $|A_0|_{exp} = 7.8 \times 10^{-4}$ cm^{-1}.

The similarity of the EPR parameters of the neutral gold complexes $[Au(^2L)(^2L^\bullet)]$ (**2**) and $[Au(mnt)(mnt^\bullet)]$ indicates only minor differences in the basis electronic structure of the two compounds. A first interpretation of the ground state can be derived from the low value of the magnetic hyperfine coupling constants. Because the isotropic part A_0 is less than 10% of that theoretically expected for the Fermi contact for

(31) A_0 only gives the s-orbital contribution and is not directly informative of the d-orbital makeup. The theoretical A_0 value for 6s gold is 1026 × 10^{-4} cm^{-1} (p 536 of Weil's 1994 book, EPR), so our measured value just tells us that we have less than 1% Au 6s. Alternatively, the contribution of the metal orbital can be estimated from the anisotropy of the *A*-tensor by using the uniaxial constant, B_0, which parameterizes the spin-dipole contribution for d-orbitals. Its theoretically value is 18.8 × 10^{-4} cm^{-1} for d^9 gold (Weil, J. A.; Bolton, J. R.; Wertz, J. E. *Electron Paramagnetic Resonance*; John Wiley & Sons, Inc.: New York, 1994; p 536). If we are to use the anistotropic *A* values from Table 4, we obtain $B = 1.3 \times 10^{-4}$ cm^{-1} and % Au (d) = 7%.
(32) Kirmse, R.; Kampf, M.; Olk, R.-M.; Hildebrand, M.; Krautscheid, H. *Z. Anorg. Allg. Chem.* **2004**, *630*, 1433.
(33) Schiødt, N. C.; Sommer-Larsen, P.; Bjørnholm, T.; Folmer-Nielsen, M.; Larsen, J.; Bechgaard, K. *Inorg. Chem.* **1995**, *34*, 3688.

Table 5. Selected Optimized Structural Parameters of Gold Complexes (Experimental Data in Parentheses)

complex	Au−S, Å	C−S, Å	C$_1$−C$_2$, Å
$[Au(^1L)_2]^{2-}$	2.410	1.780	1.362
	(2.416)^a	(1.73)	(1.37)
$[Au(^1L)_2]^{1-}$	2.362	1.788	1.359
	(2.315)^b	(1.770)	(1.355)
$[Au(^1L)(^1L^\bullet)]^0$	2.360	1.756	1.383
	(2.291)^c	(1.749)	(1.36)
$[Au(^1L^\bullet)_2]^{1+}$	2.357	1.736	1.408

^{a} From ref 32 for $[Au^{II}(mnt)_2]^{2-}$. ^{b} From this work for $[Au^{III}(^2L)_2]^-$. ^{c} From this work for $[Au(L)(L^\bullet)]$ (**2**).

a hypothetical Au(II) 5d^9 configuration,^{32} one can infer that the magnetic orbitals are having less than 10% gold 5d-character^{31} and the complexes are best described as Au(III) compounds with a ligand radical.

The frozen solution EPR spectrum of the monoanion $[Pd(^2L)(^2L^\bullet)]^-$ also shows a rhombic derivative line pattern with *g* values close to $g = 2$. Weak shoulders at the low-field lines indicate the presence of hyperfine splitting from ^{105}Pd ($I = ^5/_2$, 22.2% abundance). The spectrum was reasonably well simulated with the *g*- and *A*-values given in Table 4. The low anisotropy of both tensors as well as the low isotropic part of the magnetic hyperfine coupling again indicates predominant ligand radical character of the magnetic orbital. (Here, we refrained from simulating quadrupole effects because of the low resolution of the complex hyperfine pattern.)

Calculations. (a) Structure Optimizations. Density functional theoretical (DFT) calculations have been carried out by employing BP86 and B3LYP functionals for the dianion $[Au(^1L)_2]^{2-}$, the monoanion $[Au(^1L)_2]^{1-}$, the neutral complex $[Au(^1L)(^1L^\bullet)]^0$, and the monocation $[Au(^1L^\bullet)_2]^{1+}$, where $(^1L)^{2-}$ represents a truncated version of $(^2L)^{2-}$, the 1,2-diphenyl-ethylene-1,2-dithiolate ligand, and $(^1L^\bullet)^{1-}$ is the truncated π radical anion. Table 5 summarizes important bond distances of all of these species. The agreement of the experimental and calculated data for the monoanion and the neutral complex is reasonably good. The parameters of the ligands, in particular, are quite accurately predicted with a typical error in bond length not exceeding 0.02 Å. The overestimation of the Au−S bond distances varying 0.05−0.06 Å is typical of DFT functionals and has been observed in a variety of systems previously.^{24,34,35}

Interestingly, the optimized structures of the monoanion, the neutral complex, and the monocation feature similar Au−S bond distances at an av 2.36 Å. In contrast, the same bond in the corresponding dianion is longer at 2.41 Å. This is in excellent agreement with experiment. The Au−S bond length in $[N(n\text{-Bu})_4]_2[Au(mnt)_2]$ is reported at 2.416 Å.^{32} It

(34) (a) Bachler, V.; Olbrich, G.; Neese, F.; Wieghardt, K. *Inorg. Chem.* **2002**, *41*, 4179. (b) Lauterbach, C.; Fabian, J. *Eur. J. Inorg. Chem.* **1999**, 1995.
(35) Herebian, D.; Wieghardt, K. E.; Neese, F. *J. Am. Chem. Soc.* **2003**, *125*, 10997.
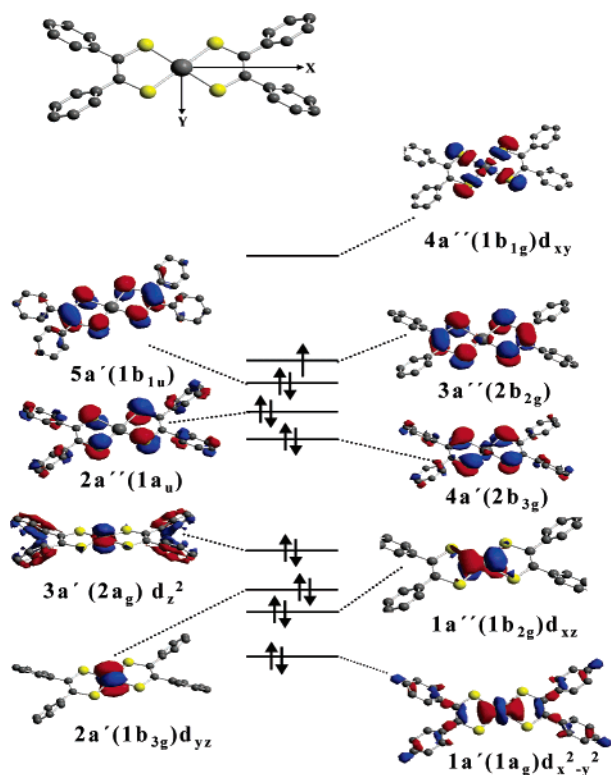
Figure 9. MO-scheme for the neutral molecule $[Au^{III}(^1L)(^1L^\bullet)]^0 \leftrightarrow [Au^{III}-(^1L^\bullet)(^1L)]^0$ as obtained from a ZORA B3LYP DFT calculation. Point group C_s is considered for this complex; in parentheses, the corresponding orbitals are labeled in D_{2h} symmetry.

is also noteworthy that the olefinic C−C bond distance increases, whereas the average C−S distance decreases on going from the monoanionic to the neutral complex and to the cation $[Au(^1L^\bullet)_2]^{1+}$. However, these metrical parameters of the ligands do not change on going from the mono- to the dianion. These findings are in excellent agreement with the notion that the one-electron-transfer steps in the series $[Au(L)_2]^{1-/0/1+}$ are ligand-based processes, whereas the reduction of the monoanion to the dianion is metal-based.

The calculated average C−S bond length in the neutral species at 1.756 Å corresponds to the arithmetic mean of the C−S bond distance at 1.788 Å in the monoanion and 1.736 Å for the monocation. Thus, the neutral complex may be described as delocalized ligand mixed valent $[Au^{III}(^1L)-(^1L^\bullet)] \leftrightarrow [Au^{III}(^1L^\bullet)(^1L)]$ (class III), whereas the monocation contains two π radical monoanions and a trivalent Au center: $[Au^{III}(^1L^\bullet)_2]^+$.

(b) Bonding Scheme and Ground-State Properties. For the MO description of the complexes within the C_s point group, we chose the coordinate system shown in Figure 9, which also exhibits a qualitative bonding scheme obtained from the spin unrestricted B3LYP DFT calculation on the neutral $[Au^{III}(^1L)(^1L^\bullet)]$ complex. The compositions of the important MOs are given in Table S1 of the Supporting Information.

The ground-state electronic configuration of $[Au^{III}(^1L)-(^1L^\bullet)]^0$ is as follows (in C_s symmetry): $(1a')^2(1a'')^2(2a')^2(3a')^2-(4a')^2(2a'')^2(5a')^2(3a'')^1(4a'')^0$.

Previously, a very similar bonding scheme[24] has been calculated for $[Au(L^{Bu})(L^{Bu\bullet})]^0$ (in D_{2h} symmetry). The Au

5d manifold lies very deep in energy due to the high effective nuclear charge of gold. Thus, the metal d and the ligand p orbitals are well separated from each other and the super-exchange interaction observed in the corresponding $[M(L^{Bu})(L^{Bu\bullet})]^{1-}$ (M = Ni, Pd, Pt) complexes[24] is reduced to a minimum. The singly occupied MO (SOMO) in $[Au^{III}-(^1L)(^1L^\bullet)]^0$ is, therefore, predominantly ligand-based with only 5% of Au $5d_{xz}$ character. In contrast, the four doubly occupied orbitals $1a'$ ($d_{x^2-y^2}$), $2a'$ (d_{yz}), $1a''$ (d_{xz}), and $3a'$ (d_{z^2}) are of mostly metal d origin, and, hence, the oxidation state of the gold ion is best represented as Au(III) (d^8).

The LUMO of the neutral complex is the antibonding combination of the metal d_{xy} and the ligand orbitals. Because of the ligand geometry, the overlap between these two orbitals is favorable, providing an efficient pathway for ligand-to-metal σ donation.

Upon one-electron reduction of $[Au^{III}(^1L)(^1L^\bullet)]^0$, the additional electron enters the $3a''$ orbital, which becomes the HOMO of the monoanion $[Au(^1L)_2]^{1-}$. Because the electron enters an orbital that is almost Au−S nonbonding, the Au−S bond length does not change upon going from the neutral to the monoanionic species. The electronic structure of the monoanion is, therefore, adequately described as a Au(III) ion attached to two closed-shell $(^1L)^{2-}$ dianions.[24,33]

Further reduction of the mono- to the corresponding dianion $[Au(^1L)_2]^{2-}$ results in the single occupancy of the $4a''$ (d_{xy}) orbital. This orbital is strongly Au−S antibonding, and, consequently, the bond length increases on going from the mono- to the dianion. The ground state of the $[Au(^1L)_2]^{2-}$ complex is calculated to be $^2A''$ with the following electron configuration: $(1a')^2(1a'')^2(2a')^2(3a')^2(4a')^2(2a'')^2(5a')^2(3a'')^2-(4a'')^1$.

This is in contrast to the suggested $^2A_{2g}$ (in D_{2h} symmetry) ground state for $[Au(mnt)_2]^{2-}$.[6] Our result supports van Rens assignment of a b_{1g} (D_{2h} symmetry) orbital symmetry of the ground state of $[Au(mnt)_2]^{2-}$ (S = $^1/_2$).[7a]

It is now interesting that the presently calculated spin population at the gold ion in $[Au(^1L)_2]^{2-}$ is significantly larger ($\sim$25%) than has been observed experimentally (10%) from a single-crystal EPR study on $[N(n\text{-}Bu)_4]_2[Au(mnt)_2]$.[7a,b] The electronic structure of the $[Au(mnt)_2]^{2-}$ dianion has previously been described in terms of a central Au(II) (d^9) attached to two closed-shell ligand dianions.[32] Based on our present calculations, it appears to be more realistic to describe the electronic structure of the dianion $[Au(^1L)_2]^{2-}$ as intermediate Au^{II}/Au^{III} with a metal−ligand delocalized SOMO (25% Au 5d, 75% 3p orbital of four S atoms). We note that previous EHT-MO calculations have also predicted a 20% Au character for this SOMO.[7b]

The electronic structure of the neutral, square-planar complexes $[Ni^{II}(L^\bullet_{X,X})_2]^0$, where $(L^\bullet_{X,X})^{1-}$ represents a semi-quinonate(1−), $(L^\bullet_{O,O})^{1-}$, an analoguous π radical anion $(L^\bullet_{N,N})^{1-}$ derived from o-phenylenediamide, or the corresponding benzene-1,2-dithiolate(1−) π radical $(L^\bullet_{S,S})^{1-}$, has recently been shown to be best described as singlet diradicals containing a diamagnetic Ni(II) ion (d^8) and two ligand π radicals, which couple antiferromagnetically yielding the observed $S_t = 0$ ground state.[34] It was shown that a single
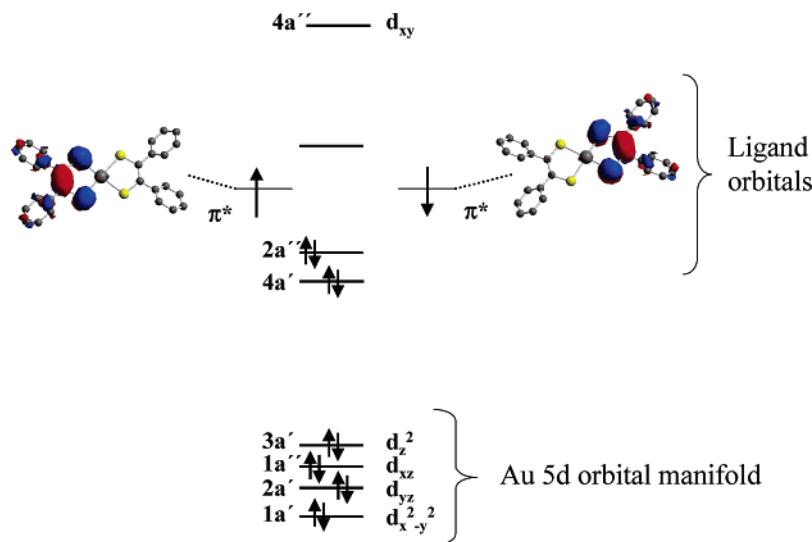
Figure 10. Qualitative MO scheme for the monocation $[Au^{III}(^1L^{\bullet})_2]^+$ as derived from a broken symmetry ZORA B3LYP DFT calculation. The doubly occupied MO's are canonical orbitals, and the singly occupied MO's result from a corresponding orbital transformation.[37] The coordinate system is the same as in Figure 9.

determinant, closed-shell approximation of the DFT method is not an appropriate starting point for a quantitative description of these complexes.[35] Therefore, the broken symmetry formalism as developed by Noodleman[36] was applied (here for the monocation $[Au(^1L^{\bullet})_2]^+$) to determine the diradical index.[24,35] The broken symmetry B3LYP wave functions of the neutral complexes show an increasing diradical character from $(L^{\bullet}_{S,S})^{1-}$, to $(L^{\bullet}_{N,N})^{1-}$ to $(L^{\bullet}_{O,O})^{1-}$. At these levels of theory, the diradical character of $[Ni^{II}(L^{\bullet}_{S,S})_2]$ is practically zero,[34a] and it does not break symmetry spontaneously. A large antiferromagnetic coupling between the two unpaired electrons of the two radical ligands is considered to be responsible for the negligible diradical character. In subsequent papers,[24,35] it was shown that the superexchange interaction through the central metal ion contributes strongly to the antiferromagnetism. The extent of the superexchange interaction depends on the effective nuclear charge of the central metal ion in the square-planar $[M(L^{\bullet}_{S,S})_2]$ complexes. Because of the small effective nuclear charge of the Ni(II) ion, the Ni d-orbitals are placed very close to the sulfur orbitals, resulting in considerable mixing of metal and ligand orbitals, and, hence, significant super-exchange interaction leading to a very small diradical character. Therefore, for $[Ni(L^{\bullet}_{S,S})_2]$, no broken symmetry solution has been found.[24,38]

On the other hand, the Au(III) ion possesses a much larger effective nuclear charge and the Au d-orbitals are situated deep in energy and are well-separated from the ligand orbitals. The antiferro-magnetic coupling between the ligand radicals mediated by the superexchange interaction through the central Au(III) ion is expected to be small. Accordingly, a broken symmetry solution has been found for the mono-cation $[Au^{III}(^1L^{\bullet})_2]^{1+}$. A qualitative bonding scheme derived

(36) (a) Noodleman, L. *J. Chem. Phys.* **1981**, *74*, 5737. (b) Noodleman, L.; Davidson, E. R. *Chem. Phys.* **1986**, *109*, 131.
(37) Neese, F. *J. Phys. Chem. Solids* **2004**, *65*, 781.
(38) Lim, B. S.; Fomitchev, D. V.; Holm, R. H. *Inorg. Chem.* **2001**, *40*, 4257.

Table 6. Comparison of the Charge and Spin Populations at the Gold Ion As Calculated from a Natural Population Analysis of the One-Electron Density of the Ground State Obtained from Scalar Relativistic ZORA-B3LYP DFT Calculations

complex	electron-5d	electrons-6s	spin-5d
$[Au(^1L)_2]^{2-}$	9.34	0.62	0.25
$[Au(^1L)_2]^{1-}$	8.91	0.58	0.00
$[Au(^1L)(^1L^{\bullet})]^0$	8.89	0.60	0.05
$[Au(^1L^{\bullet})_2]^{1+}$	8.84	0.64	0.00

from such a B3LYP broken symmetry DFT calculation is shown in Figure 10 for this species. There are six doubly occupied canonical MOs, four of which are of predominantly Au character and are situated very low in energy (Au(III), d^8). The remaining two orbitals are at higher energy and ligand-based. Analysis of the corresponding orbitals[37] yields a spin-coupled (magnetic) pair formed between two ligand-based orbitals. The overlap between these two orbitals is 0.35. A diradical character of 88% is calculated by using proce-dures described in ref 33 with a singlet−triplet ($-2J_{GS}$) gap of 1024 cm^{-1}. The electronic structure of $[Au(III)(^1L^{\bullet})_2]^{1+}$ can therefore be described in terms of a central, diamagnetic Au(III) ion (d^8) attached to two antiferromagnetically coupled ligand π radicals.

Interestingly, similar calculations performed on the iso-electronic complex $[Pd^{II}(^1L^{\bullet})_2]$ did not produce a broken symmetry solution. Because of the lower effective nuclear charge of Pd(II) as compared to Au(III), the Pd orbitals are situated closer in energy to the ligand-based orbitals. A Pd d-orbital contribution of ~20% has been calculated for the SOMO (HOMO).

Table 6 gives the results of a natural population analysis of the B3LYP densities for the gold complexes. Interestingly, the d population remains constant in the series $[Au(^1L)_2]^{1+/0/1-}$ but changes significantly upon reduction to the dianion. This is again consistent with ligand-based electron-transfer pro-cesses in the above series of complexes and a significant metal contribution to the SOMO in the dianion.

Table 7. Calculated (Experimental Data in Parentheses) EPR Parameters As Obtained from the Scalar Relativistic ZORA-B3LYP DFT Calculations

complex	g_x	g_y	g_z	A_x, MHz	A_y, MHz	A_z, MHz
$[Au(^1L)(^1L^\bullet)]^0$	2.028	2.023	1.962	−10	−15	−11
$[Au(^2L)(^2L^\bullet)]^a$	(2.065)	(2.030)	(1.944)	(−20)	(−20)	(−19)
$[Au(mnt)(mnt^\bullet)]^{0\,a}$	(2.0758)	(2.0381)	(1.9279)	(−16)	(−91)	(−24)
$[Au(^1L)_2]^{2-}$	2.08	2.05	2.00	−203	−204	−193
$[Au(mnt)_2]^{2-\,b}$	(2.02)	(2.01)	(1.98)	(−123)	(−121)	(−119)

^{a} This work. ^{b} Reference 7.

Table 8. Results of the ZORA-B3LYP TD-DFT Calculation on $[Au^{III}(^1L)(^1L^\bullet)] \leftrightarrow [Au^{III}(^1L^\bullet)(^1L)]$

	energy, cm^{-1}		oscillator strength	
transition (C_s)	exp.	calc.	exp.	calc.
$5a' \rightarrow 3a''$	6666	7020	0.129	0.20
$2a' \rightarrow 3a''$	7800	7300	0.025	0.03

(c) Calculation of EPR Parameters. The calculated EPR parameters (ZORA-B3LYP DFT level) are summarized in Table 7. The calculated g-values and ^{197}Au hyperfine splitting parameters of $[Au^{III}(^1L)(^1L^\bullet)] \leftrightarrow [Au^{III}(^1L^\bullet)(^1L)]$ are in reasonable agreement with the experimental ones for $[Au^{III}(^2L)(^2L^\bullet)] \leftrightarrow [Au^{III}(^2L^\bullet)(^2L)]$ (see above). The SOMO of this species is predominantly ligand-based with only 5% of Au d$_{xz}$ character. Consequently, together with the rather small nuclear moment of the ^{197}Au nucleus, the ^{197}Au hyperfine constants are small, both calculated and experimental. There is also little angular momentum in the ground-state wave function, and, thus, the calculated and observed g-shifts are small and reflect the organic radical character of the ground state.

On the other hand, large ^{197}Au ($I = \frac{3}{2}$, 100% natural abundance) hyperfine splittings are predicted by calculations for the dianionic complex $[Au^{II}(^1L)_2]^{2-}$. The experimental spectrum of $[Au^{II}(^1L)_2]^{2-}$ has not been measured due to its instability in solution. However, the EPR parameters for $[Au(mnt)_2]^{2-\,7b}$ given in Table 7 agree reasonably well with those calculated for $[Au^{II}(^1L)_2]^{2-}$.

(d) Excited-State Calculations. The electronic spectra of the $[M(L^{Bu})_2]^{0/1-/2-}$ (M = Ni, Pd, Pt) and of $[Au(L^{Bu})_2]^{0/1-}$ complexes have been reported previously in detail.[5,24]

Assuming D_{2h} symmetry, the $1b_{1u} \rightarrow 2b_{2g}$ transition in the $[M(L^{Bu})(L^{Bu\bullet})]^z$ complexes is predominantly ligand-to-ligand intervalence charge transfer (IVCT) in origin and is assigned to the intense band in the NIR region. For the diradical complexes $[M(L^\bullet)_2]^z$, the $1b_{1u} \rightarrow 2b_{2g}$ transition is ligand-to-ligand charge transfer (LLCT) in origin and also occurs in the NIR region. As pointed out above, the intensity of the LLCT band is approximately twice that of the IVCT band.

The calculated spectra of complexes as obtained from time-dependent DFT calculations are in reasonable agreement with experiment as shown in Table 8. For the neutral $[Au(^1L)(^1L^\bullet)]^0$ complex, the most intense transition in the NIR region is an IVCT band and corresponds to the 5a' (1b$_{1u}$ in D_{2h}) $\rightarrow$ 3a'' (2b$_{2g}$ in D_{2h}) transition. It is predicted at 7020 cm^{-1} and is observed at 6666 cm^{-1}. The next transition is calculated at 7300 cm^{-1} with a smaller oscillator strength.

This is assigned to a 2a' (1a$_u$ in D_{2h}) $\rightarrow$ 3a'' (2b$_{2g}$ in D_{2h}) transition, which is experimentally observed at 7800 cm^{-1} (oscillator strength 0.025).

For the two $[Au(^1L)_2]^{1-/2-}$ species, the 3a'' (2b$_{2g}$ in D_{2h}) orbital is doubly occupied, and, consequently, no transitions are calculated in the NIR in agreement with experiment. Note that the 2a' (1a$_u$ in D_{2h}) $\rightarrow$ 4a'' (1b$_{1g}$ in D_{2h}) transition expected for all three species, $[Au(L)_2]^{0/1-/2-}$, appears at high energy and is not observed in the first 25 calculated states (energy range 5000−25 000 cm^{-1}) of these complexes.

As pointed out previously,[35] the broken symmetry formalism only crudely models the multireference character of the diradical system $[M(L^\bullet)_2]^n$ and is not an entirely satisfactory substitute for a genuine multiconfigurational treatment. Hence, no TD-DFT calculations were performed on the $[Au(^1L^\bullet)_2]^{1+}$ complex.

Summary

The principal results of this investigation are summarized as follows.

(1) For the first time, a four-membered, reversible electron-transfer series $[Au(L)_2]^z$ ($z = 1+$, 0, 1−, and 2−) has been characterized electrochemically and, in part, chemically. Similarly, the three-membered, reversible series $[Pd(L)_2]^z$ ($z = 0$, 1−, 2−) has also been investigated. All members possess a planar structure (C_s symmetry).

(2) By using DFT calculations at the B3LYP level, the geometries of the above gold series $[Au(^1L)_2]^z$ with $z = 1+$, 0, 1−, 2− and of $[Pd^{II}(^1L^\bullet)_2]^0$ have been optimized and compared to experimental X-ray data where possible. Agreement is in general excellent. The observed trends in Au−S, C−S, and C−C distances within the series are reliably reproduced. Calculated EPR parameters for paramagnetic $[Au^{III}(^1L^\bullet)(^1L)]^0 \leftrightarrow [Au^{III}(^1L)(^1L^\bullet)]$ and $[Au^{II}(^1L)_2]^{2-}$ are also in excellent agreement with experiment. The electronic spectrum of the above neutral species has also been calculated, and, again, the data are in excellent agreement with experiment.

(3) From these calculations, it is clearly established that four doubly occupied, energetically low lying metal d-orbitals exist, which allow the assignment of an Au(III) (d^8) oxidation state for the monocation, the neutral, and the monoanionic gold species. Two molecular orbitals at significantly higher energy can then be identified as being the electroactive orbitals 5a' (in C_s) or 1b$_{1u}$ (D_{2h} symmetry) and 3a'' (in C_s) or 2b$_{2g}$ (in D_{2h}), which are predominantly ligand-based. Thus, independent of the overall charge z, these two orbitals have 0% and only 5% metal d-character, respectively. This is in contrast to the corresponding series $[Ni(S_2C_2Me_2)_2]^{0,1-,2-}$, where the 2b$_{2g}$ orbital has a much higher metal d-character ($\sim$20%).[38] Similarly, the corresponding DFT calculations for $[Pd(^1L^\bullet)_2]^0$ show that the HOMO 3a'' has $\sim$20% metal character. It is thus clear that the redox steps for $[Au(^1L)_2]^z$ ($z = 1+$, 0, 1−) are nearly purely ligand-based. For the monocation $[Au^{III}(^1L^\bullet)_2]^+$, a diradical character of 88% has been calculated from a broken symmetry DFT calculation again in contrast to calculations on the corresponding neutral

complexes of Ni[34,38] and Pd for which no broken symmetry solutions were found.

Supporting Information Available: X-ray crystallographic files for compounds **1**, **2**, and **4**, and Table S1 containing the composition of selected molecular orbitals of [Au(^{1}L)$_2$]^z complexes. This material is available free of charge via the Internet at http://pubs.acs.org.

IC061181U